Available online at www.eccomasproceedia.org
Eccomas Proceedia COMPDYN (2023) 3017-3027

ECCOMAS
Proceedia

COMPDYN 2023
9th ECCOMAS Thematic Conference on
Computational Methods in Structural Dynamics and Earthquake Engineering
M. Papadrakakis, M. Fragiadakis (eds.)
Athens, Greece, 12-14 June 2023

STATIC AND DYNAMIC EXPERIMENTAL VALIDATIONS OF THE LATERAL IMPACT RESILIENT DOUBLE CONCAVE FRICTION PENDULUM (LIR-DCFP) BEARING

G. Auad[1], P. Castaldo[2], J. L. Almazán[1], and D. Quizanga[1]

[2] Department of Structural Engineering, Pontificia Universidad Católica de Chile
Avenida Vicuña Mackenna, 4860, Santiago, Chile
{gaauad, jlalmaza, dmquizanga}@uc.cl

[2] Department of Structural, Geotechnical and Building Engineering (DISEG), Politecnico di Torino
Corso Duca degli Abruzzi, 24, Torino, Italy
paolo.castaldo@polito.it

Abstract

During high-magnitude earthquakes, large base displacements that exceed the lateral capacity of the isolation level can cause internal impacts jeopardizing the benefits of using seismic isolation. The Lateral Impact Resilient Double Concave Friction Pendulum (LIR-DCFP) bearing has been proposed to mitigate the adverse effects of internal lateral impacts between inner sliders and restraining rims of sliding surfaces. This device has an enhanced inner slider formed by two bodies. These bodies are in contact, generating a plane high-friction interface capable of dissipating additional energy and limiting the magnitude of the impact. A numerical model based on rigid body dynamics has been proposed to represent the dynamic response of structures equipped with LIR-DCFP bearings. The numerical formulation includes important modeling aspects such as lateral impact behavior and large displacements (P-Δ effects), among other essential phenomena. A prototype of this novel device was constructed to validate its lateral behavior through static experimental tests. As predicted, if the inner slider does not contact the restraining rims of the sliding surfaces, the response of the isolator will be identical to the response of the classical frictional isolators. On the contrary, for larger lateral displacements, the contact between the inner slider and the restraining rims triggers high friction sliding. Finally, experimental tests were conducted to validate the dynamic response of a stiff structure equipped with four LIR-DCFP devices. An accurate prediction of the dynamic response can be obtained by employing the suggested numerical model under the presence or absence of internal lateral impacts.

Keywords: Seismic isolation, LIR-DCFP bearing, internal lateral impact, high-friction interface.

ISSN:2623-3347
Peer-review under responsibility of the organizing committee of COMPDYN 2023.
doi: 10.7712/120123.10619.20298

1 INTRODUCTION

Friction Pendulum System (FPS) bearings [1] are commonly used to achieve seismic isolation, protecting superstructures from high-magnitude earthquakes. Particularly, the FPS device consists of an articulated slider and one plate with a spherical sliding surface. A restraining rim is placed on the plate to limit the maximum base displacement. Several alternatives exist to construct isolation levels using frictional isolators with multiple sliding surfaces. Two of the most used devices with multiple sliding surfaces are the Double Concave Frictional Pendulum (DCFP) [2] and Triple Concave Friction Pendulum (TCFP) [3,4] bearings. The presence of more than one sliding surface allows a passive adaptive behavior to be generated. In this way, it is possible to change both damping and stiffness properties based on different base displacement demands. All the cited devices have shown excellent seismic performance [2,3,5–7].

Under extreme ground motions, large base displacement could cause internal lateral impacts between inner sliders and restraining rims. Internal impacts can produce an critical rise in the ductility demand of the superstructure [8–13] or the failure of the DCFP and TCFP isolators [14,15].

A new frictional isolator, called the Lateral Impact Resilient Double Concave Friction Pendulum (LIR-DCFP) bearing, has been suggested to mitigate the adverse effects of internal impacts [16–18]. This device has an improved inner slider with a high friction interface. The sliding in this interface starts when the inner slider impacts the restraining rims of the concave plates, dissipating an additional amount of energy and limiting the magnitude of the impact force. Numerical evaluations of the seismic performance of structures equipped with LIR-DCFP bearings have been conducted to determine the comparative advantages of using the novel friction bearing instead of classical isolation devices [16–18].

The first part of this paper presents a static experimental validation of the lateral behavior of the LIR-DCFP bearing is presented. This experimental test aims to determine if the hysteretic response obtained by imposing cyclic lateral displacements is consistent with the expected theoretical response.

The second part of this research aims to validate a numerical model based on rigid body dynamics developed by Auad & Almazán [16]. The numerical formulation includes important modeling aspects such as lateral impact behavior, large displacements ($P-\Delta$ effects), uplifting, bi-directional frictional coupling, and kinematics constraints, among other essential phenomena. Dynamic tests were conducted applying sinusoidal ground motions to generate experimental data valuable to validate the dynamic response of a numerical model of the tested base-isolated structure.

2 LATERAL BEHAVIOR OF THE LIR-DCFP BEARING

2.1 Geometric description

The Lateral Resilient Double Concave Friction Pendulum (LIR-DCFP) isolator has been suggested as an alternative to mitigate the adverse effects of impacts between inner sliders and restraining rims of frictional devices [16–18]. Typically, this isolator consists of two plates with spherical sliding surfaces characterized by a radius of curvature R. Between the concave plates, an enhanced inner slider is located. This slider is the key feature of the new device. The inner slider is composed of two bodies: the upper slider and the bottom slider. Both pieces are in contact, generating a planar high-friction interface. On the one hand, low friction contacts (between the spherical surfaces of the slider and the sliding surfaces) are typified by a low friction coefficient μ_d that depends on the sliding velocity $\dot{v}$ according to the following equation [5,6]:

$$\mu_d = f_{max} - (f_{max} - f_{min})\exp(-\alpha \dot{v}) \quad (1)$$

being, f_{max} and f_{min} the friction coefficient at a high and slow velocity, respectively, and α the rate parameter. On the other hand, the planar high friction contact between the upper and bottom sliders is assumed to be independent of the sliding velocity and denoted by the symbol μ_h. In Figure 1, a schematic illustration of the LIR-DCFP bearing is presented, indicating the name of the components and the region where slow and high friction interactions are generated.

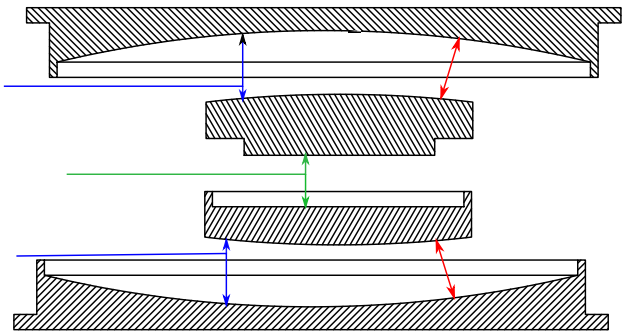

Figure 1: Illustration of the LIR-DCFP bearing.

The mechanism created to mitigate the adverse effects of internal lateral impacts consists of triggering the high friction sliding when the inner slider contacts the restraining rims of the concave plates. This condition is satisfied by ensuring in the design steps that $\mu_h > \mu_d$. If high friction sliding occurs, the magnitude of the impact force will be limited, and a critical amount of energy will be dissipated. In Figure 2, the expected lateral behavior in terms of normalized force-displacement relationship is shown, including different deformed configurations of the device.

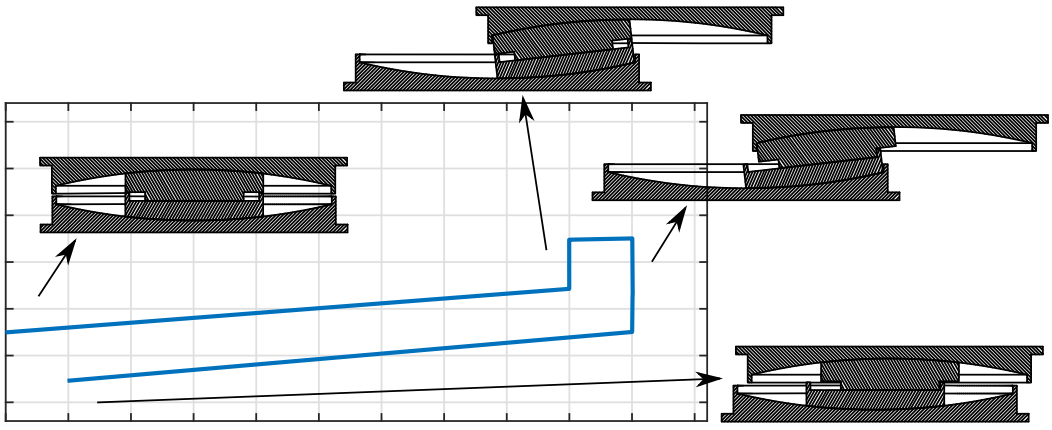

Figure 2: Expected lateral behavior of the LIR-DCFP bearing.

2.2 Experimental hysteretic validation of the LIR-DCFP bearing.

This subsection presents the main results of a cyclic static experimental test. This test was conducted to validate the expected lateral behavior of the novel device. The experimental setup is presented in Figure 3(a). While an axial load of 150 kN is applied using a horizontally

orientated actuator, the displacement of the bottom plate of the isolator is imposed employing a vertically orientated hydraulic actuator. Two constant velocity cycles with an amplitude of 18.5 cm were imposed on the prototype. The tested device has two identical sliding surfaces with a radius of curvature equal to $R = 0.75$ m. Since the inner slider has a height of 8.5 cm, the effective radius of curvature of the isolator is equal to $R_{eff} = 1.415$ m [2]. While the low friction interactions are defined by a friction coefficient of $\mu_d = 0.066$, the developed friction coefficient of the planar interface between the top and bottom slider was equal to $\mu_h = 0.126$.

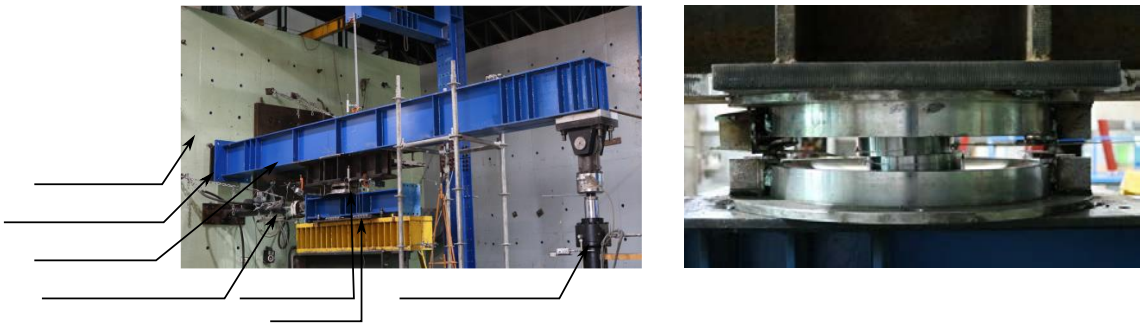

Figure 3: (a) Experimental setup; (b) Prototype of the LIR-DCFP bearing.

In Figure 4, the obtained normalized hysteretic loops that characterize the lateral behavior of the LIR-DCFP bearing are presented. As predicted, the displacement of the device starts with low friction sliding between spherical surfaces. The first high friction sliding is triggered by the impact between the inner slider and the restraining rims of the plates at a lateral displacement of 17.5 cm. Note that the magnitude of the impact force is limited to the force needed to overcome the sticking phase of the high-friction interface. Also, an additional amount of energy is dissipated during the planar sliding. This first high-friction sliding generates a relative displacement between the top and bottom sliders of 1 cm, explaining why the second high-friction sliding occurs for a displacement of 16.5 cm.

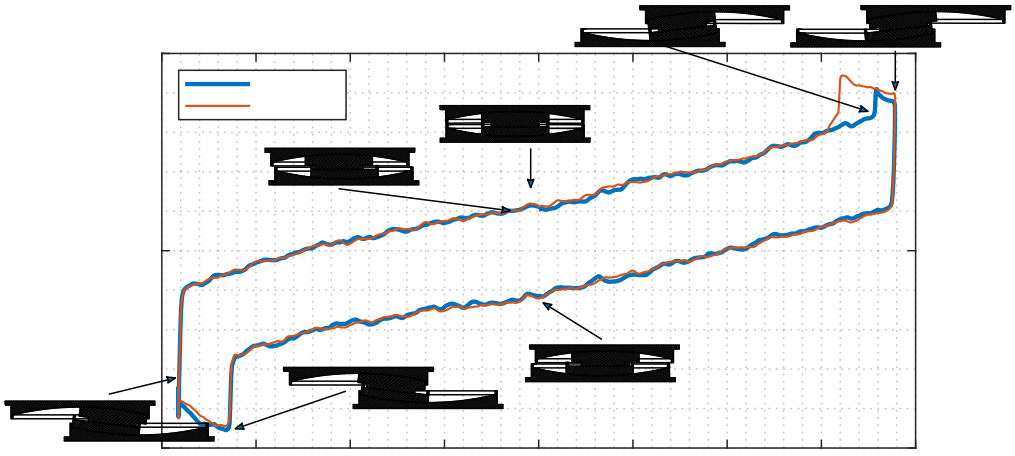

Figure 4: Experimental hysteretic loops.

3 NUMERICAL FORMULATION OF THE LIR-DCFP BEARING

In this Section, the numerical formulation of the LIR-DCFP bearing is briefly described. A complete report can be found in [16]. The three-dimensional modeling procedure is based on rigid body dynamics and was proposed by Bao and Becker [19]. The first step is to define a set of contact and projection points. As an example, in Figure 5, four pairs contact-projection points are defined for each interaction between bodies that form the isolator. The contact between the upper slider and the upper plate is considered using the pairs $A_i - A_i'$. The contact between the bottom slider and the bottom plate is included using the pairs $B_j - B_j'$. Finally, the high friction interaction between the slider is modeled using the points $C_k - C_k'$. Since contact points are located in a rigid body, it is possible to track their global location and velocity by knowing the displacements and velocities of the centroid of the rigid bodies and the angular velocity of the pieces that form the isolator. Suppose the position and velocity of all the contact and projection points are known. In that case, it is possible to determine the contact forces generation between the interaction of the rigid bodies. As an example, the interaction force of one generic couple $B_j - B_j'$ in local coordinates can be computed by determining the normal force N_{B_j} and the two components of the friction force $\boldsymbol{f_{\mu,A_1}} = [\, f_{\mu,A_1}^{(x)};\, f_{\mu,A_1}^{(y)} \,]$ using the following equations:

$$N_{B_j} = \begin{Bmatrix} k\left(\boldsymbol{r_{B_j}}(3) - \boldsymbol{r'_{B_j}}(3)\right) + c\left(\dot{\boldsymbol{r}}_{\boldsymbol{B_j}}(3) - \dot{\boldsymbol{r}}'_{\boldsymbol{B_j}}(3)\right), if\left(\boldsymbol{r_{B_j}}(3) - \boldsymbol{r'_j}(3)\right) \geq 0 \\ 0, \text{ otherwise} \end{Bmatrix} \quad (2)$$

$$\boldsymbol{f_{\mu,B_j}} = -\mu_d N_{B_j} \boldsymbol{z_{B_j}} \quad (3)$$

in which $\boldsymbol{r_{B_j}}$ and $\boldsymbol{r'_{B_j}}$ are the position of the contact and projection point, respectively; and $\dot{\boldsymbol{r}}_{\boldsymbol{B_j}}$ and $\dot{\boldsymbol{r}}'_{\boldsymbol{B_j}}$ are the velocities of the contact and projection point, respectively. Note that the normal force is computed by employing a Kelvin-Voigth element [20], being k and c, the stiffness and damping coefficient of the element. The friction phenomenon is modeled using the well-known biaxial Bouc-W ' , $\boldsymbol{z_{B_j}}$ the vector that contains the two hysteretic parameters associated with the pair $B_j - B_j'$. Both forces can be arranged in a three-dimension vector as follows:

$$\boldsymbol{f_{n,B_j}} = [N_{B_j};\, \boldsymbol{f_{\mu,B_j}}] \quad (4)$$

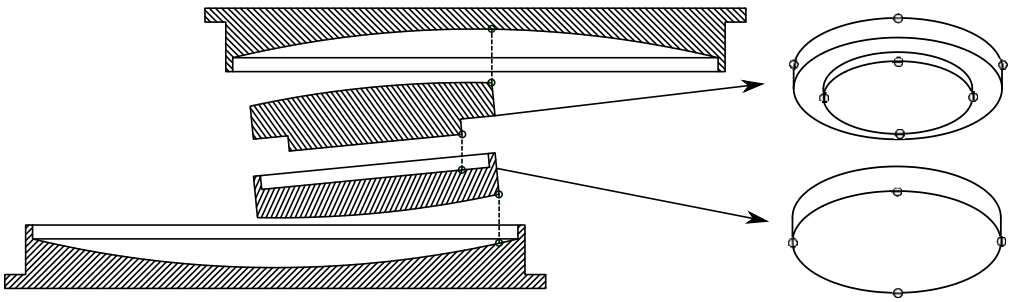

Figure 5: Location of a set of four contact-projection points for each interaction [16].

The vectorial force presented in Equation (4) is described in local coordinates. All the contact forces (external force according to the procedure) in local coordinates can be rotated to global coordinates. By considering the contribution of all the contact forces in global coordinates, it is possible to determine the generalized vector as follows:

$$\boldsymbol{F} = \sum_n \frac{\partial \boldsymbol{r_c}}{\partial \boldsymbol{q}} \cdot \boldsymbol{f_n} + \sum_n \left((\boldsymbol{r_n} - \boldsymbol{r_c}) \times \boldsymbol{f_n} \right) \cdot \frac{\partial \bar{\boldsymbol{\omega}}}{\partial \boldsymbol{q}} \tag{5}$$

where, the symbol $\boldsymbol{f_n}$ denotes the nth contact force described in global coordinates; $\boldsymbol{r_c}$ is the vector from the origin of the global system to the centroid of the considered rigid body; and $\bar{\boldsymbol{\omega}}$ is the angular velocity vector of the considered rigid body. Assuming that the bottom plate is connected to the ground, there are three rigid bodies that can be displaced. Since a three-dimensional formulation is used, the motion of each rigid body can be described by 6 degrees of freedom (i.e., three displacements and three rotations), leading to a total of 18 degrees of freedom. The vector that contains the 18 degrees-of-freedom is denoted by the symbol $\boldsymbol{q}$.

3.1 Numerical model example

In this Subsection, the dynamic response of a LIR-DCFP bearing with sliding surfaces with a radius equal to $R = 1.185$ m and a slider with a height of $h = 0.12$ m (i.e., effective radius of $R_{eff} = 2.25$ m) is presented. The impact between the inner slider and the restraining rims of the sliding plate is produced if the base displacement exceeds 0.25 m. The low friction interactions are characterized by the following parameters: $f_{max} = 0.065$, $f_{min} = f_{max}/2$, and $\alpha = 15$ sec/m. The high-friction interface is defined by a constant friction coefficient of $\mu_h = 2f_{max}$. A lumped mass of $m_s = 204$ kN×sec^2/m was assigned to the top plate of the bearing. The numerical model was subjected to one horizontal component of the Newhall record (Northridge earthquake, 1994).

The motion of the bearing is presented in Figure 6. The displacements of the bodies that are not connected to the ground are shown in Figure 6(a). Note that the impact is observed at $t = 4.2$ sec, triggering the high friction sliding. This sliding is noticeable since a relative displacement between the bottom and top slider is generated. The numerical formulation is based on rigid dynamics. In this way, by adopting a large value of the stiffness in the contact-projection points interaction, the kinematic constraints of describing a spherical trajectory are satisfied. In Figure 6(b), the vertical displacement of the components of the LIR-DCFP isolator is shown, confirming that a vertical displacement accompanies a lateral displacement. The numerical formulation allows even to include the rotation. This response is presented in Figure 6(c).

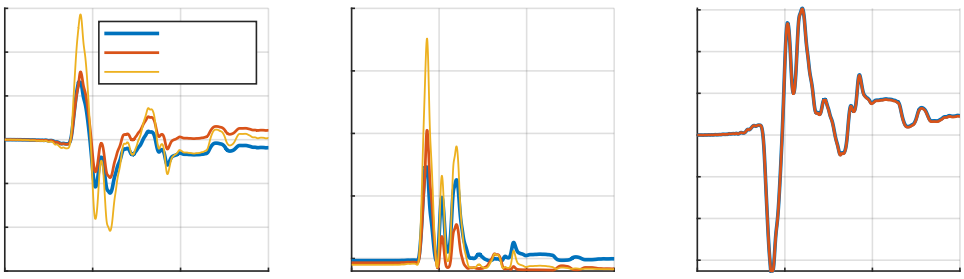

Figure 6: Dynamic Response of the numerical formulation of a LIR-DCFP bearing: (a) Lateral displacements; (b) Vertical displacements; (c) Rotations.

The configurations of the different bodies that form the isolator are depicted in Figure 7. In this figure, it is possible to check the position of the plates and sliders before, during, and after the impact.

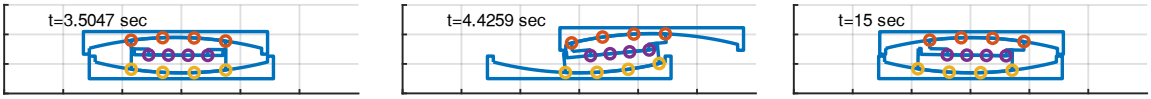

Figure 7: Deformed configurations of a LIR-DCFP bearing: (a) Before the impact; (b) During the impact; (c) After the impact.

The response of the isolator in terms of forces transmitted to the superstructure is presented in Figure 8. The lateral force generated in the device is presented in Figure 8(a). It is noticeable that even when the impact occurs ($t = 4.2$ sec), the magnitude of the lateral force does not present a dramatic increase but only increases until the high friction interface slides. The described numerical formulation allows including $P - \Delta$ effects, phenomenon that is critical when large displacements are expected. Figure 8(b) shows the evolution of the bending moment that the isolator transfers to the superstructure. The hysteric lateral response of the LIR-DCFP can be seen in Figure 8(c). The high friction sliding occurs when the lateral capacity of the bearing is exceeded. If the slider impacts the restraining rims of the plates, an additional amount of energy is dissipated.

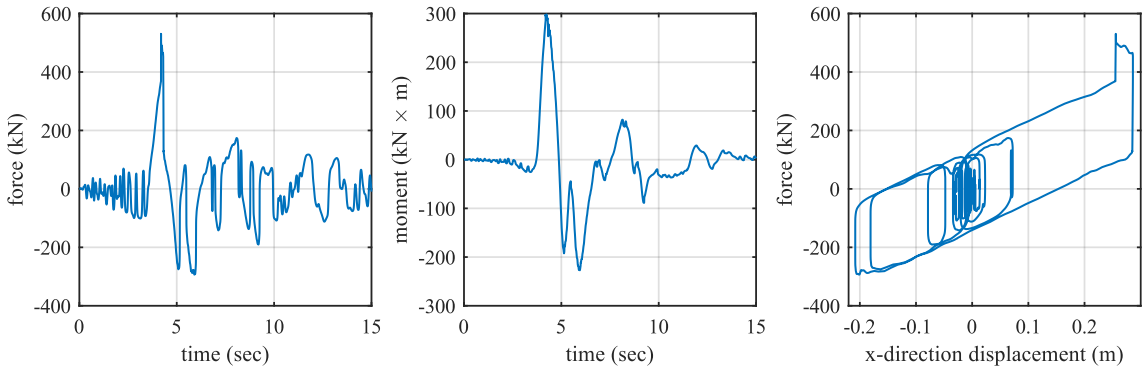

Figure 8: Dynamic Response of the numerical formulation of a LIR-DCFP bearing: (a) Lateral force; (b) Moment; (c) Hysteretic loops.

4 DYNAMIC VALIDATION OF THE LIR-DCFP LATERAL BEHAVIOR

A small-scaled stiff two stories structure equipped with four LIR-DCFP isolators was built to validate the dynamic response of the isolation system. In Figure 9, the base-isolated structure and one LIR-DCFP isolator are shown. The isolators that form the flexible level were characterized by the following parameters: radius of curvature $R = 0.75$ m, slider height $h = 0.05$ m, a lateral capacity of 0.11 m, maximum and minimum friction coefficient in the low friction interaction of $f_{max} = 0.14$ and $f_{min} = 0.11$, and a high friction coefficient in the high friction interface of $\mu_h = 0.27$. The total seismic weight acting on the isolation system was $W_{sis} = 26.6$ kN.

Figure 9: (a) Experimental setup of the dynamic tests; (b) LIR-DCFP bearing used in the dynamic tests.

Periodic waves were imposed on the dynamic system in one direction using a horizontal actuator. The objective of these tests was to validate the expected response of the isolation system under two conditions: (i) with internal lateral impacts and (ii) without internal lateral impacts. Periodic accelerations with different amplitudes were applied to observe both conditions. The input generated using the shaking table was measured to have the data to replicate the tests numerically. These signals are shown in Figure 10.

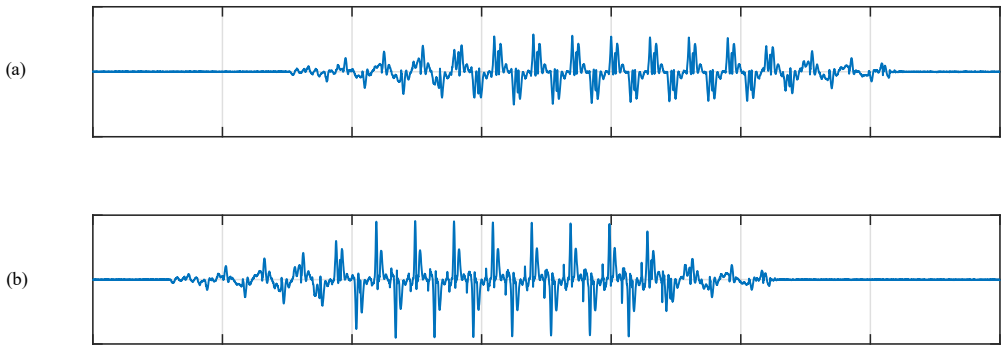

Figure 10: Experimental seismic inputs: (a) Test without impacts; (b) Test with impacts.

A numerical model of the base-isolated structure was developed in the MATLAB environment. The isolation devices were modeled employing the numerical formulation described in this work. A comparison between the experimental and numerical dynamic response of the isolation system is shown in Figure 11 in terms of base displacement and hysteretic loops generated in the isolation system. In Figure 11(a, b), the response without impacts is plotted. Note that since impacts between the inner slider and the restraining rims do not occur, high friction sliding is not generated. In this case, as expected, the dynamic behavior of the isolation system is equal to a classic isolation interface formed by DCFP bearings. In Figure 11(c, d), the dynamic response of the isolation system, including the lateral impact behavior, is presented. Similar responses are obtained, indicating that the developed numerical model can be an excellent tool to predict the response of an isolation system with LIR-DCFP bearing. A good match between the experimental and numerical response in terms of the maximum response of the base displacement and total base shear of the isolation system is obtained. It is essential to highlight that even in the presence of lateral internal impacts, the maximum base shear does not exceed the 60% of the seismic weight. Furthermore, the isolation devices can resist several high-

friction relative displacements between the top and bottom sliders. The use of LIR-DCFP bearing can be an effective way of mitigating the adverse effects of internal lateral impacts.

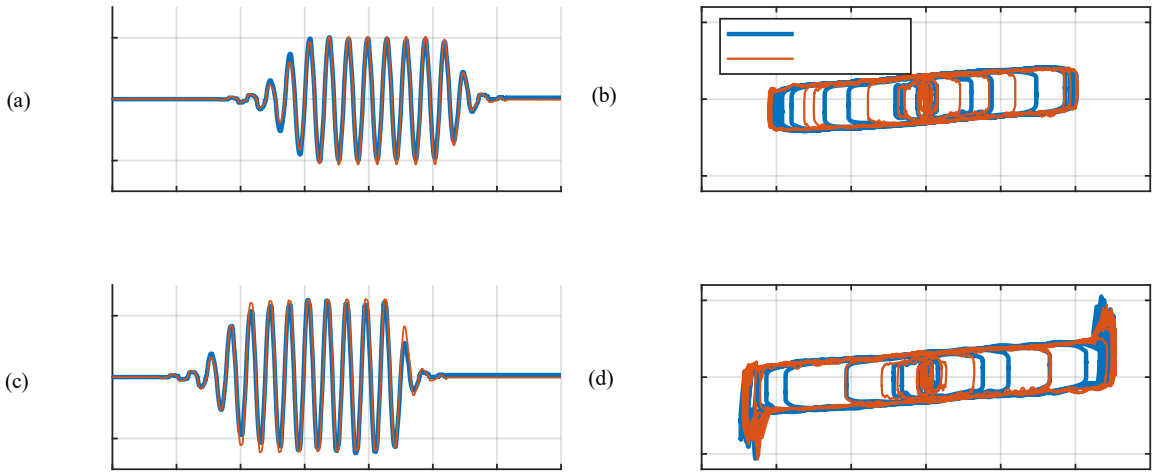

Figure 11: Comparison of the experimental and numerical response of the isolation system: (a) Base displacement without impacts; (b) Hysteretic loops without impacts; (c) Base displacement with impacts; (d) Hysteretic loops with impacts.

5 CONCLUSIONS

This paper presents an experimental validation of the constructability and lateral behavior of the Lateral Impact Resilient Double Concave Friction Pendulum (LIR-DCFP) bearing. This device has been suggested to mitigate the adverse effects of internal impacts between inner sliders and restraining rims of frictional isolators. The main advantage of the LIR-DCFP device over classical frictional bearings is its high friction interface. This interface allows to limit the impact force and dissipating an additional amount of energy during the internal lateral impact.

A static test of an LIR-DCPF prototype was conducted to validate the hysteretic behavior of the isolator. As expected, since the friction interaction in the high-friction interface is characterized by a friction coefficient larger than the friction coefficient generated between spherical surfaces, high-friction sliding occurs when the slider impacts the restraining rims of the concave plates. This static test indicates that the idea of creating a high-friction interface is feasible.

Dynamics tests were conducted to generate data on the response of an isolation system formed by four LIR-DCFP bearings. This data was used to validate a numerical model of the device. This numerical formulation is based on rigid body dynamics and includes essential modeling aspects such as lateral impact behavior, large displacements, $P-\Delta$ effects, among other phenomena. The numerical model of the novel device is able to accurately predict the dynamic response of the isolation system under the presence or absence of internal lateral impacts. Additionally, the responses obtained from the dynamic tests of the base-isolated structure indicate that this new technology can effectively mitigate the adverse effects of internal lateral impacts.

REFERENCES

[1] V.A. Zayas, S.S. Low, S.A. Mahin, A Simple Pendulum Technique for Achieving

Seismic Isolation, Earthq. Spectra. 6 (1990) 317–333. https://doi.org/10.1193/1.1585573.

[2] D.M. Fenz, M.C. Constantinou, Behaviour of the double concave Friction Pendulum bearing, Earthq. Eng. Struct. Dyn. 35 (2006) 1403–1424. https://doi.org/10.1002/eqe.589.

[3] D.M. Fenz, M.C. Constantinou, Spherical sliding isolation bearings with adaptive behavior: Theory, Earthq. Eng. Struct. Dyn. 37 (2008) 163–183. https://doi.org/10.1002/eqe.751.

[4] D.M. Fenz, M.C. Constantinou, Modeling triple friction pendulum bearings for response-history analysis, Earthq. Spectra. 24 (2008) 1011–1028. https://doi.org/10.1193/1.2982531.

[5] A. Mokha, M. Constantinou, A. Reinhorn, Teflon Bearings in Base Isolation I: Testing, J. Struct. Eng. 116 (1990) 438–454. https://doi.org/10.1061/(ASCE)0733-9445(1990)116:2(438).

[6] M. Constantinou, A. Mokha, A. Reinhorn, Teflon Bearings in Base Isolation II: Modeling, J. Struct. Eng. 116 (1990) 455–474. https://doi.org/10.1061/(ASCE)0733-9445(1990)116:2(455).

[7] D.M. Fenz, M.C. Constantinou, Spherical sliding isolation bearings with adaptive behavior: Experimental verification, Earthq. Eng. Struct. Dyn. 37 (2008) 185–205. https://doi.org/10.1002/eqe.750.

[8] Y. Bao, T.C. Becker, Inelastic response of base-isolated structures subjected to impact, Eng. Struct. 171 (2018) 86–93. https://doi.org/10.1016/j.engstruct.2018.05.091.

[9] Y. Bao, T.C. Becker, T. Sone, H. Hamaguchi, To limit forces or displacements: Collapse study of steel frames isolated by sliding bearings with and without restraining rims, Soil Dyn. Earthq. Eng. 112 (2018) 203–214. https://doi.org/10.1016/j.soildyn.2018.05.006.

[10] Y. Bao, T.C. Becker, Effect of Design Methodology on Collapse of Friction Pendulum Isolated Moment-Resisting and Concentrically Braced Frames, J. Struct. Eng. 144 (2018) 04018203. https://doi.org/10.1061/(asce)st.1943-541x.0002183.

[11] E.A. Mavronicola, P.C. Polycarpou, P. Komodromos, Spatial seismic modeling of base-
s :
and mass eccentricity, (2017) 1161–1179. https://doi.org/10.1002/eqe.

[12] P.C. Polycarpou, P. Komodromos, Earthquake-induced poundings of a seismically isolated building with adjacent structures, Eng. Struct. 32 (2010) 1937–1951. https://doi.org/10.1016/j.engstruct.2010.03.011.

[13] P. Komodromos, Simulation of the earthquake-induced pounding of seismically isolated buildings, Comput. Struct. 86 (2008) 618–626. https://doi.org/10.1016/j.compstruc.2007.08.001.

[14] Y. Bao, T.C. Becker, H. Hamaguchi, Failure of double friction pendulum bearings under pulse-type motions, Earthq. Eng. Struct. Dyn. 46 (2017) 715–732. https://doi.org/10.1002/eqe.2827.

[15] T.C. Becker, Y. Bao, S.A. Mahin, Extreme behavior in a triple friction pendulum isolated frame, Earthq. Eng. Struct. Dyn. 46 (2017) 2683–2698. https://doi.org/10.1002/eqe.2924.

[16] G. Auad, J.L. Almazán, Lateral Impact Resilient double concave Friction Pendulum

(LIR-DCFP) bearing: Formulation, parametric study of the slider and three-dimensional numerical example, Eng. Struct. 233 (2021). https://doi.org/10.1016/j.engstruct.2021.111892.

[17] G. Auad, P. Castaldo, J.L. Almazán, Seismic reliability of structures equipped with LIR-DCFP bearings in terms of superstructure ductility and isolator displacement, Earthq. Eng. Struct. Dyn. 51 (2022) 3171–3214. https://doi.org/10.1002/eqe.3719.

[18] G. Auad, Mitigating the adverse effects of internal lateral impacts in structures equipped with frictional isolators, Pontificia Universidad Católica de Chile, 2022.

[19] Y. Bao, T. Becker, Three-dimensional double friction pendulum bearing model including uplift and impact behavior: Formulation and numerical example, Eng. Struct. 199 (2019) 109579. https://doi.org/10.1016/j.engstruct.2019.109579.

[20] S.A. Anagnostopoulos, Equivalent viscous damping for modeling inelastic impacts in earthquake pounding problems, Earthq. Eng. Struct. Dyn. 33 (2004) 897–902. https://doi.org/10.1002/eqe.377.